ELSEVIER

Gas-phase synthesis of hydroxyacetophenones by acylation of phenol with acetic acid

C.L. Padró, C.R. Apesteguía *

Catalysis Science and Engineering Research Group (GICIC), Instituto de Investigaciones en Catálisis y Petroquímica–INCAPE (UNL-CONICET), Santiago del Estero 2654, 3000 Santa Fe, Argentina

Abstract

The gas-phase synthesis of aromatic ketones via acylation of phenol with acetic acid was studied on SiO_2–Al_2O_3, Al-MCM-41, zeolites HY and ZSM5, and tungstophosphoric acid (HPA) supported on MCM-41 and carbon. At contact times of 146 g h/mol, the initial conversion of phenol varied between 12.5% (HY) and 19.1% (HPA/MCM-41), and the initial selectivity to *ortho*-hydroxyacetophenone (*o*-HAP) between 37.1% (HPA/C) and 69.1% (HY). In all the cases, the formation of *o*-HAP was clearly favored in comparison to that of *para*-isomer. Zeolites HY and ZSM5, which contained strong Brønsted and Lewis acid sites, produced efficiently *o*-HAP via both the direct C-acylation of phenol and the acylation of phenyl acetate intermediate formed from O-acylation of phenol. HPA-based catalysts contained only Brønsted acid sites and formed *o*-HAP exclusively as a secondary product from phenyl acetate. The *o*-HAP yield remained constant with time on stream on ZSM5 but drastically decreased on the other samples because of coke formation. The superior stability of zeolite ZSM5 was interpreted by considering that coke precursor formation is avoided into the microporous structure of this zeolite.

1. Introduction

Aromatic ketones are valuable intermediate compounds for the synthesis of important pharmaceuticals and fragrances. In particular, *ortho*- (*o*-HAP) and *para*-hydroxyacetophenone (*p*-HAP) are widely used for the synthesis of aspirin and paracetamol (4-acetoaminophenol), respectively [1]. *o*-Hydroxyacetophenone is a key intermediate for producing 4-hydroxycoumarin and warfarin which are both used as anticoagulant drugs in the therapy of thrombotic disease [2], and it has been also employed for obtaining flavonones [3,4]. Hydroxyacetophenones are commercially produced via the Fries rearrangement of phenyl acetate in a liquid-phase process involving the use of Lewis and Brønsted acids, such as $AlCl_3$, $TiCl_4$, $FeCl_3$, and HF, which pose problems of high toxicity, corrosion, and spent acid disposal [5]. Recently, it was reported that the Fries rearrange-

ment of phenyl acetate to *p*-HAP is efficiently catalyzed by methane sulfonic acid, a strong and biodegradable acid [6]. In general, the liquid-phase Fries rearrangement of phenyl acetate forms mainly *p*-HAP, giving *p*-HAP/*o*-HAP ratios between 2 and 8, but also produces significant amounts of phenolic by-products. Considerable research work has been performed recently to find suitable, recyclable, and environmentally benign solid acid catalysts for efficiently promoting the liquid-phase synthesis of aromatic ketones from phenyl acetate. Strong solid acids such as ion-exchange resins, zeolites, Nafion, and heteropoly acids show moderate phenyl acetate conversion activity and preferentially produce *p*-HAP, but also give significant amounts of phenol and are in general rapidly deactivated because of the formation of ketene byproducts that are highly reactive coke intermediates [7–11].

Hydroxyacetophenones are also obtained by the acylation of phenol using acid halides [12] or acid anhydrides [13] as acylating agents. In the liquid phase, the reaction is catalyzed by Friedel–Crafts catalysts and produces mainly *p*-HAP, although the isomer selectivity may be changed by changing the solvent polarity. In the gas phase, the acylation of phe-

* Corresponding author. Fax: 54 342 4531068.
  E-mail address: capesteg@fiqus.unl.edu.ar (C.R. Apesteguía).
  URL: http://www.ceride.gov.ar/gicic .

ARTICLE IN PRESS

S0021-9517(04)00288-X/FLA AID:8348 Vol.226(2)
ELSGMLTM(YJCAT):m5 2004/05/28 Prn:28/06/2004; 13:34

yjcat8348

P.309 (308-320)
by:Jolanta p. 2

C.L. Padró, C.R. Apesteguía / Journal of Catalysis 226 (2004) 308–320   309

Scheme 1. *para*- and *ortho*-HAP formation from the acylation of phenol with acetic acid.

nol with acetic acid or acetic anhydride has been carried out on Al-MCM-41 and zeolite ZSM5, at temperatures between 520 and 573 K [14–19]. Scheme 1 shows the synthesis of p- and o-HAP from the acylation of phenol with acetic acid. It was found that the gas-phase phenol acylation on solid acids forms predominantly o-HAP, giving o-HAP/p-HAP molar ratios higher than 80 [14,16]. However, the experimental o-HAP yields were moderate, particularly because of the significant formation of phenyl acetate [18,19]. The reaction network of the gas-phase acylation of phenol with acetic acid was studied by Neves et al. [17], but more detailed studies are needed to ascertain the exact requirements of acid site density and strength to efficiently promote the selective o-HAP formation. Our understanding of the deactivation mechanism under reaction conditions is also lacking, despite the fact that the potential use of solid acids in gas-phase acylation reactions is often limited because of the rapid activity decay caused by coke formation.

In this paper, we perform a detailed study of the gas-phase acylation of phenol with acetic acid over different solid acids. Specifically, we prepared and characterized HPA/MCM-41, Al-MCM-41, zeolites HY and ZSM5, HPA/carbon, and SiO$_2$–Al$_2$O$_3$ catalysts. Our goal was to relate the structural properties and the surface acid site density and strength of the solids with their ability for the efficient catalysis of the phenol acylation reaction to yield o-HAP. Results will show that zeolite ZSM5 does not deactivate on stream and produces selectively o-HAP at high rates. The unique performance of zeolite ZSM5 is based on its high density of strong Lewis and Brønsted acid sites that promote the formation of o-HAP both by direct C-acylation of phenol and by phenyl acetate obtained from O-acylation of phenol, and on its microporous structure that hinders the formation coke precursor intermediates.

2. Experimental

2.1. Catalyst preparation

Pure silica MCM-41 and Al-MCM-41 mesoporous materials were synthesized according to Edler and White [20].

Sodium silicate solution (14% NaOH and 27% SiO$_2$, Aldrich), cetyltrimethylammonium bromide (Aldrich), aluminum isopropoxide (Aldrich), and deionizated water were used as the reagents. The composition of the synthesis gel was 7SiO$_2$–x Al$_2$O$_3$–2.7Na$_2$O–3.7CTMABr–1000H$_2$O. The pH was adjusted to 10 using a 0.1 M H$_2$SO$_4$ solution, and then the gel was transferred to a Teflon-lined stainless-steel autoclave and heated to 373 K in an oven for 96 h. After crystallization, the solid was washed with deionized water, dried at 373 K, and finally calcined at 773 K for 4 h. HPA/MCM-41 was prepared following the procedure of Kozhenikov et al. [21] by stirring a suspension of 1 g of MCM-41 in 30 cm^3 of an aqueous solution of HPA (H$_3$PW$_{12}$O$_{40}$·6H$_2$O, Merck) at room temperature for 24 h. After evaporation of the solvent at 333 K under vacuum, the solid was dried at 353 K and calcined in air at 573 K. HPA/C was prepared by stirring a suspension of carbon (from Westvaco) in a hydrochloric HPA solution at pH 1.6 for 24 h. The HY zeolite was prepared by triple ion exchange of a commercial NaY zeolite (UOP-Y 54) with ammonium acetate (Sigma, 99%) at 298 K and subsequent calcination in air. The H form of ZSM5 zeolite (Zeocat Pentasil PZ-2/54) was obtained following the same procedure used for HY. SiO$_2$–Al$_2$O$_3$ (Ketjen LA-LPV) was calcined at 773 K.

2.2. Catalyst characterization

The crystalline structures of MCM-41, Al-MCM-41, HPA/C, and HPA/MCM-41 were determined by X-ray diffraction (XRD) using a Shimadzu XD-D1 diffractometer and Ni-filtered Cu$K\alpha$ radiation. BET surface areas (S_g), mean pore diameter ($\bar{d}_p$), and pore-size distribution were measured by N$_2$ physisorption at its boiling point in a Quantochrome Corporation NOVA-1000 sorptometer. Elemental compositions were measured by atomic absorption spectroscopy (AAS).

Acid site densities were determined by temperature-programmed desorption (TPD) of NH$_3$ preadsorbed at 373 K. Samples (200 mg) were treated in He (60 cm^3/min) at 773 K for 1.5 h and then exposed to a 1% NH$_3$/He stream for 40 min at 373 K. Weakly adsorbed NH$_3$ was removed by

yjcat8348

C.L. Padró, C.R. Apesteguía / Journal of Catalysis 226 (2004) 308–320

flowing He at 373 K for 2 h. The temperature was then increased at 10 K/min and the NH_3 concentration in the effluent was measured by mass spectrometry (MS) in a Baltzers Omnistar unit.

The nature of surface acid sites was determined by Fourier transform infrared spectroscopy (FT-IR) by using pyridine as probe molecule and a Shimadzu FTIR-8101M spectrophotometer. The spectral resolution was 4 cm^{-1} and 50 scans were coadded. Sample wafers were formed by pressing 20–40 mg of the catalyst at 5 tons/cm^2 and transferred to a sample holder made of quartz. An inverted T-shaped Pyrex cell containing the sample pellet was used. The two ends of the short arm of the T were fitted with CaF_2 windows. All the samples were initially outgassed at 723 K for 4 h and then a background spectrum was recorded after cooling the sample at room temperature. Data were obtained after admission of pyridine, adsorption at room temperature, and sequential evacuation at 298, 423, 573, and 723 K. Spectra were always recorded at room temperature. Difference spectra were obtained by substracting the background spectrum recorded previously.

Coke formed on the catalysts during reaction was measured by temperature-programmed oxidation (TPO). Samples (50 mg) were heated in a 3% O_2/N_2 stream at 10 K/min from room temperature to 1073 K. The evolved CO_2 was converted to methane by means of a methanation catalyst (Ni/kieselghur) operating at 673 K and monitored using a flame ionization detector.

2.3. Catalytic testing

The gas-phase acylation of phenol (Merck, > 99%) with acetic acid (Merck, 99.5%) was carried out in a fixed-bed, continuous-flow reactor at 553 K and 101.3 kPa. Samples were sieved to retain particles with 0.35–0.42 mm diameter for catalytic measurements and pretreated in air at 773 K for 2 h before reaction, except samples containing HPA that were pretreated in air at 573 K for 2 h. Phenol (P) and acetic acid (AA) were introduced (P/AA = 1) via a syringe pump and vaporized into flowing N_2 to give a $N_2/(P + AA)$ ratio of 45. Standard catalytic tests were conducted at a contact time (W/F_P^0) of 146 g h/mol and gas-hour space velocity (GHSV) of 235 cm^3 STP/(g min). The exit gases were analyzed on-line using a Hewlett-Packard 5890 chromatograph equipped with a Supelcowax 10 column and a flame ionization detector. Data were collected every 25 min for about 6 h. The main products of phenol acylation with acetic acid were phenyl acetate (PA), *ortho*-hydroxyacetophenone (*o*-HAP) and *para*-hydroxyacetophenone (*p*-HAP); *para*-acetoxyacetophenone (*p*-AXAP) was detected in trace amounts. Phenol conversion $(X_P, $ mol of phenol reacted/mol of phenol fed) was calculated as: $X_P = \sum Y_i/(\sum Y_i + Y_P)$, where $\sum Y_i$ is the molar fraction of products formed from phenol, and Y_P is the outlet molar fraction of phenol. The selectivity to product i $(S_i,$ mol of product i/mol of phenol reacted) was determined as:

Table 1
Chemical composition and physical properties of the catalysts used in this work

Samples	Surface area S_g (m^2/g)	Pore diameter $\bar{d}_P$ (Å)	Si/Al	HPA (%)
HY	660	7.4	2.4	–
NaY	700	7.4	2.4	–
ZSM5	350	5.5	20	–
SiO_2–Al_2O_3	560	45	11.3	–
Al-MCM-41	925	30	18	–
MCM-41	1010	34	∞	–
Carbon	1700	22	–	–
HPA	6	–	–	100
HPA/C	390	30	–	28
HPA/MCM-41	505	29	–	30

S_i (%) = $[Y_i/\sum Y_i]100$. Product yields (η_i, mol of product i/mol of phenol fed) were calculated as $\eta_i = S_i X_P$.

3. Results and discussion

3.1. Catalyst characterization

The physicochemical characteristics (surface area, pore diameter, chemical composition) of the samples used in this work are summarized in Table 1. BET surface areas of MCM-41 and carbon samples are higher than 1000 m^2/g. However, after impregnation with HPA the S_g values dropped to 505 (HPA/MCM-41) and 390 m^2/g (HPA/C). In the case of carbon, the HPA molecules blocked the carbon micropore structure and, as a consequence, the average pore diameter increased from 22 to 30 Å. In contrast, the HPA addition to MCM-41 did not change the support pore diameter size, probably because MCM-41 exhibits a uniformly sized mesoporous structure.

XRD patterns of Al-MCM-41 and MCM-41 samples showed that both samples are well crystallized and exhibit a strong diffraction peak at 2.2° corresponding to 100 reflection; no other crystalline phases were observed. On the other hand, no crystalline HPA structure was detected on HPA-supported samples, thereby indicating that the HPA phase is well dispersed on MCM-41 and carbon supports.

Sample acid properties were probed by TPD of NH_3 preadsorbed at 373 K. The obtained TPD curves are shown in Fig. 1. The NH_3 surface densities for acid sites were obtained by deconvolution and integration of TPD traces and are presented in Table 2. The NH_3 evolved from MCM-41 and carbon supports was negligible. The acid site strength of HPA-based samples was clearly higher compared to the other samples. Pure HPA showed a sharp NH_3 desorption peak at about 910 K, which accounts for the strong Brønsted acid sites present on this material. This high-temperature desorption peak was also detected on HPA/C and HPA/MCM-41 samples, which presented an additional low-temperature peak at ca. 493 K. The evolved NH_3 from HY, ZSM5, and SiO_2–Al_2O_3 samples gave rise to
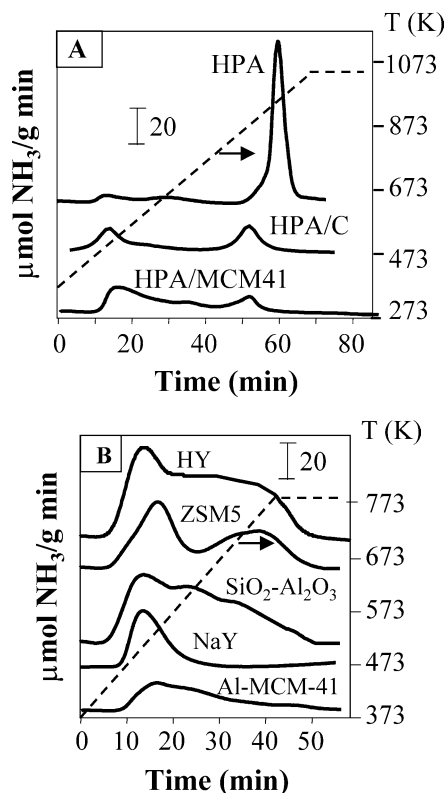
ARTICLE IN PRESS

S0021-9517(04)00288-X/FLA AID:8348 Vol.226(2)
ELSGMLTM(YJCAT):m5 2004/05/28 Prn:28/06/2004; 13:34

yjcat8348

P.311 (308-320)
by:Jolanta p. 4

311

Fig. 1. TPD profiles of NH$_3$ on: (A) HPA-based samples; (B) SiO$_2$–Al$_2$O$_3$, Al-MCM-41, and acid zeolites. Heating rate: 10 K/min.

Table 2
Characterization of sample acidity: TPD of NH$_3$ and FTIR of pyridine

Catalyst	TPD of NH$_3$		FTIR of pyridine		
	(µmol/g)	(µmol/m^2)	Brønsted sites (B) (area/g)	Lewis sites (L) (area/g)	L/B
HY	1380	2.1	310	465	1.5
NaY	280	0.4	n.d.[a]	525	–
ZSM5	770	2.2	337	341	1.0
SiO$_2$–Al$_2$O$_3$	1005	1.8	68	204	3.0
Al-MCM-41	340	0.4	32	135	4.2
HPA	539	90.0	–	–	–
HPA/C	315	0.8	–	–	–
HPA/MCM-41	352	0.7	–	–	–

[a] n.d., not detected.

a peak at 483–493 K and a broad band between 573 and 773 K. In contrast, zeolite NaY desorbed NH$_3$ in a single TPD peak centered at about 480 K. On a weight basis, the HY zeolite exhibited the highest surface acid density (1380 µmol/g), probably reflecting the higher aluminum content, followed by SiO$_2$–Al$_2$O$_3$ (1005 µmol/g) and ZSM5 (770 µmol/g) samples. For the other samples, the amount of evolved NH$_3$ was between 550 and 280 µmol/g. Pure HPA presented the highest acid site density on an areal basis (90.0 µmol/m^2), followed by zeolites ZSM5 (2.2 µmol/m^2) and HY (2.1 µmol/m^2).

Fig. 2 shows the FT-IR spectra in the hydroxyl stretching region of SiO$_2$–Al$_2$O$_3$, Al-MCM-41, NaY, ZSM5, and
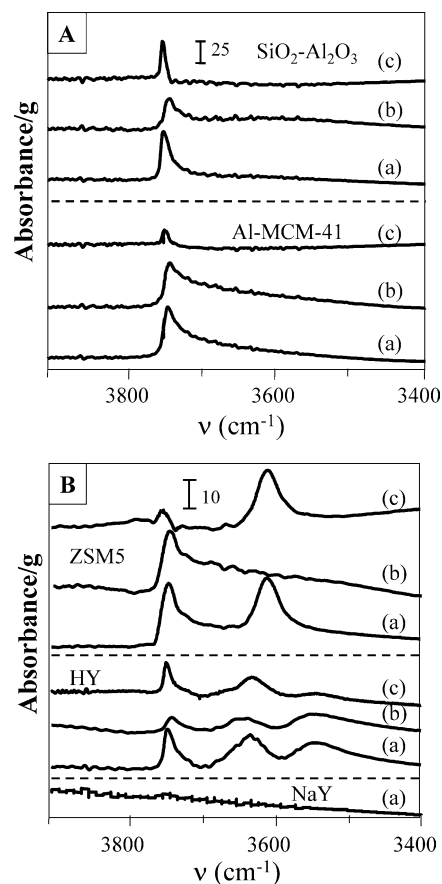
Fig. 2. FT-IR spectra in the hydroxyls stretching region of: (A) SiO$_2$–Al$_2$O$_3$ and Al-MCM-41; (B) NaY, ZSM5, and HY. (a) Degassed at 723 K for 4 h; (b) after pyridine adsorption at room temperature and desorption at 423 K for 0.5 h; (c) difference spectra (a)–(b).

HY samples obtained after evacuation at 723 K for 4 h, and after pyridine adsorption at room temperature and desorption at 423 K for 0.5 h. Difference spectra are also included. The position of the IR band for the O–H stretching modes (ν_{OH}) over degassed Al-MCM-41 and SiO$_2$–Al$_2$O$_3$ is almost the same, about 3745 cm^{-1} (Fig. 2A), but the ν_{OH} wavenumber on oxides is not directly related to the acid strength of the hydroxyl group [22]. More useful information on Brønsted acid site strength is obtained by analyzing the difference spectra in Fig. 2A. It is observed, in fact, that after desorption at 423 K of the pyridine adsorbed at room temperature, the base is almost completely eliminated on Al-MCM-41 but remains adsorbed to a significant extent on SiO$_2$–Al$_2$O$_3$. This result reflects the stronger acidity of surface OH groups on SiO$_2$–Al$_2$O$_3$ compared to Al-MCM-41. On the other hand, no absorption bands were detected in the hydroxyl stretching on the NaY sample (Fig. 2B), thereby indicating that the hydroxyl group concentration on this zeolite is negligible. The spectrum of degassed zeolite ZSM5 shows two absorption bands at 3610 and 3745 cm^{-1}, respectively. The band at 3610 cm^{-1} corresponds to Si–OH–Al bridging hydroxyl groups [23] whereas the asymmetric band at 3745 cm^{-1} is attributed to the stretching

vibration of terminal SiOH groups located either at the boundaries of the zeolite crystal or at the surface of non-crystalline material [24]. Fig. 2B shows that evacuation at 423 K does not remove to any extent the pyridine adsorbed at room temperature on bridging OH at 3610 cm^{-1}, reflecting the strong adsorption of pyridine on Si–OH–Al groups of zeolite ZSM5. In contrast, the interaction of pyridine with terminal silanol OH groups at 3745 cm^{-1} is very weak. Finally, the IR spectrum of zeolite HY matrix shows three absorption bands which correspond to high-frequency Si–OH–Al groups (3620 cm^{-1}), low-frequency Si–OH–Al groups (3550 cm^{-1}), and terminal silanol groups (3743 cm^{-1}) [25]. Difference spectra in Fig. 2B show that pyridine strongly adsorbs on high-frequency Si–OH–Al groups associated to OH groups located in large cavities. The low-frequency band at 3550 cm^{-1} attributed to OH groups in the sodalite cages is less affected by pyridine adsorption. Very weakly acidic SiOH groups at 3743 cm^{-1} are also affected by pyridine adsorption, probably because of a perturbation of these groups by the pyridine molecules adsorbed on neighboring Lewis sites [26].

The density and nature of surface acid sites were determined from the FT-IR spectra of adsorbed pyridine. Fig. 3A shows the spectra obtained on zeolite HY after admission

of pyridine, adsorption at room temperature, and sequential evacuation at 298, 423, 573, and 723 K. The pyridine absorption bands at around 1540 cm^{-1} and between 1440 and 1460 cm^{-1} arise from pyridine adsorbed on Brønsted and Lewis acid sites, respectively, on zeolites [27–30], Al-MCM-41 [30,31], and SiO$_2$–Al$_2$O$_3$ [32]. Fig. 3A shows that the spectrum collected following evacuation at 298 K contains broad absorption bands, characteristic of the presence of physisorbed pyridine. Pyridine molecules interacting via H bonding with weakly acidic surface OH groups (bands at 1446 and 1597 cm^{-1}) are removed after evacuation at 423 K and the resulting FT-IR spectrum shows well-defined absorption peaks. We decided then to characterize the sample acidity by using spectra collected after evacuation at 423 K. Fig. 3B compares the FT-IR spectra obtained on samples HY, NaY, ZSM5, Al-MCM-41, and SiO$_2$–Al$_2$O$_3$ after pyridine evacuation at 423 K. The relative contributions of Lewis and Brønsted acid sites were obtained by deconvolution and integration of pyridine absorption bands appearing in Fig. 3B at around 1450 and 1540 cm^{-1}, respectively. Results are given in Table 2. In general, the band at 1540 cm^{-1} characteristic for pyridinium ions does not change in wavenumber upon varying the sample acidity but the frequency of the band accounting for coordinately bound pyridine increases with the strength of interaction [22]. FT-IR spectra of Fig. 3B show that on Al-MCM-41 and SiO$_2$–Al$_2$O$_3$ samples the coordinately bound pyridine band appears at 1455 cm^{-1}, which reflects the adsorption of pyridine on Lewis acid sites associated with tricoordinate Al atoms. In agreement with the results obtained by TPD of NH$_3$, the amount of pyridine adsorbed on Al-MCM-41 after evacuation at 423 K is clearly lower compared to acid zeolites or SiO$_2$–Al$_2$O$_3$, reflecting the moderate acidic character of mesoporous Al-MCM-41 sample. On the other hand, the areal peak relationship between Lewis and Brønsted sites, L/B, was higher on Al-MCM-41 than on SiO$_2$–Al$_2$O$_3$ (Table 2). The relative density of Brønsted and Lewis acid sites on Al-MCM-41 depends, of course, on the Si/Al ratio, but the value of L/B = 4.2 determined for our Si/Al = 18 sample is close to that reported for Al-MCM-41 samples containing similar Si/Al ratios [31]. Consistent with the IR characterization of hydroxyl groups in Fig. 2, the pyridine absorption spectrum on zeolite NaY does not reveal the presence of surface Brønsted sites. The band representing Lewis acid centers appears on NaY at 1443 cm^{-1}, a frequency considerable lower compared to those determined for similar bands on Al-MCM-41 and SiO$_2$–Al$_2$O$_3$ samples. This frequency shift has been interpreted by considering that the pyridine is adsorbed on NaY by a polarization of the molecule in the field due to cation [28]; i.e., the interaction is associated with Na rather than to Al. Fig. 3A shows that on zeolite HY the pyridine absorption bands associated with Brønsted and Lewis acid sites appear after evacuation at 423 K at 1542 and 1454 cm^{-1}, respectively. These two bands are present even after evacuation of zeolite HY at 723 K, thereby indicating that zeolite HY contains strong Brønsted and Lewis acid sites. But it

Fig. 3. FT-IR spectra of pyridine adsorbed on: (A) zeolite HY at 298 K and evacuated at increasing temperatures; (B) SiO$_2$–Al$_2$O$_3$, Al-MCM-41, and acid zeolites at 298 K and evacuated 423 K for 0.5 h. Dotted lines indicate the presence of Lewis (1450 cm^{-1}) and Brønsted (1540 cm^{-1}) sites.

ARTICLE IN PRESS
S0021-9517(04)00288-X/FLA   AID:8348   Vol.226(2)
ELSGMLTM(YJCAT):m5 2004/05/28 Prn:28/06/2004; 13:34

yjcat8348

P.313 (308-320)
by:Jolanta p. 6

C.L. Padró, C.R. Apesteguía / Journal of Catalysis 226 (2004) 308–320   313

should be noted that the L/B ratio on HY increases with the evacuation temperature from 1.5 (423 K) to 2.2 (723 K). The increase of the L/B ratio with the desorption temperature on zeolite HY has already been reported [26] and probably reflects the fact that a part of the Brønsted sites corresponding to the bridged hydroxyl groups of the structure are of medium strength. Nevertheless, some of the Brønsted sites display strong acidity, as evidenced by the FTIR data. These stronger Brønsted sites are associated either to bridged OH interacting with the Lewis sites or to extraframework OH groups [33]. The very strong Lewis sites of zeolite HY have been associated [26] with aluminum atoms that are either extraframework (tetracoordinated) or associated with framework defects (tricoordinated). On zeolite ZSM5, the band of adsorbed pyridine on Lewis acid sites is split in two overlapping peaks at 1445 and 1455 cm^{-1}, respectively. A similar two-peak band for the pyridine adsorption on Lewis acid sites on ZSM5 was reported from researchers of the Mobil Company [34]. These authors suggested [34] that the Lewis acidity on ZSM5 is due to Al located in the zeolite framework, probably generated during calcination, resulting in partial hydrolysis of Al–O bonds. Zeolite ZSM5 contained a similar concentration of Brønsted and Lewis acid sites (Table 2), but in contrast to zeolite HY the ratio L/B did not vary significantly by increasing the desorption temperature of adsorbed pyridine. It was determined, in fact, that after degassing at 723 K the L/B ratio was 0.92 that was similar to that measured following evacuation at 423 K (L/B = 1.0).

3.2. Catalytic testing

Fig. 4A shows phenol conversion (X_P) and product selectivities (S_i) obtained at 553 K on zeolite HY and typically illustrates the time-on-stream behavior of the catalysts during the reaction. It is observed that the phenol conversion practically remained unmodified but the product selectivity significantly changed during the catalytic test. The PA selectivity increased with time on stream at the expense of the formation of *ortho* and *para*-HAP isomers. On the other hand, the formation of *o*-HAP compared to that of *p*-HAP was highly favored. Qualitatively, a similar catalytic behavior on stream was observed for the other samples, excepting ZSM5. In fact, as it is shown in Fig. 4B, on ZSM5 not only X_P but also the product selectivities did not change with time on stream.

The conversion and selectivity values obtained for all the samples at times zero and 4 h are given in Table 3. Values at time zero were obtained by extrapolating to zero the time-on-stream curves using semilogarithmic plots. Zeolite HY showed the highest initial selectivity values to *o*-HAP and *p*-HAP (69 and 8.9%, respectively), but after 4 h of reaction the *o*-HAP selectivity decreased to only 10.4%. Zeolite NaY also produced ab initio predominantly *o*-HAP, but did not form *p*-HAP and the phenol conversion diminished significantly on stream. Pure HPA and HPA/MCM-41 were among the most active catalysts and efficiently converted phenol to
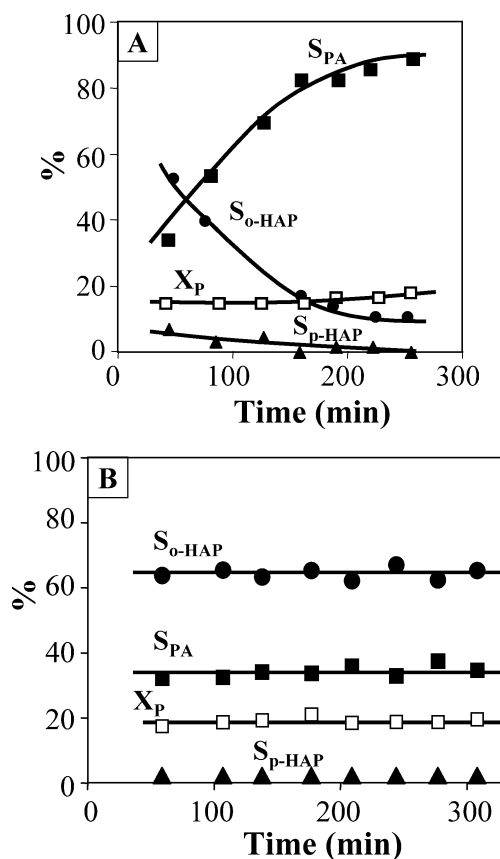

Fig. 4. Phenol conversion and product selectivities as a function of time on stream on: (A) zeolite HY; (B) zeolite ZSM5 [553 K, 101.3 kPa total pressure, $W/F_P^0 = 146$ g h/mol, P/AA = 1, $N_2/(P + AA) = 45$].

Table 3
Phenol conversion (X_P), selectivities to *o*-HAP ($S_{o\text{-HAP}}$), *p*-HAP ($S_{p\text{-HAP}}$), and PA (S_{PA}), at times zero and 4 h

Catalysts	$t = 0$ h				$t = 4$ h			
	X_P^0	$S_{o\text{-HAP}}^0$	$S_{p\text{-HAP}}^0$	S_{PA}^0	X_P	$S_{o\text{-HAP}}$	$S_{p\text{-HAP}}$	S_{PA}
HY	15.0	69.1	8.9	22.0	15.4	10.4	1.4	88.2
NaY	15.9	62.0	–	38.0	8.1	8.1	–	91.9
ZSM5	18.2	67.1	0.2	32.7	18.2	65.3	–	34.7
Al-MCM-41	12.9	52.3	1.2	46.5	13.1	30.9	1.0	68.1
SiO$_2$–Al$_2$O$_3$	16.0	39.1	1.6	58.3	15.9	21.9	1.1	76.4
HPA	22.3	21.0	1.6	77.5	24.3	2.4	0.5	96.3
HPA/C	15.3	37.0	1.5	61.0	15.5	15.8	0.9	83.3
HPA/MCM-41	19.1	52.0	–	48.0	21.7	2.6	–	97.4

$T = 553$ K, $W/F_P^0 = 146$ g h/mol; P/AA = 1, $N_2/(P + AA) = 45$.

PA, but they rapidly lost their ability for producing the *o*-HAP isomer. The HPA/C sample was more stable for *o*-HAP formation and after 4 h on stream still exhibited a nonnegligible $S_{o\text{-HAP}}$ value (15.8%). SiO$_2$–Al$_2$O$_3$ and Al-MCM-41 were more stable than HPA-based catalysts for *o*-HAP formation; in particular, it is noted that the $S_{o\text{-HAP}}$ value on Al-MCM-41 was 30.9% after 4 h on stream. But the most stable catalyst was zeolite ZSM5; actually, we did not observe on ZSM5 sample any significant activity decay for the *o*-HAP formation rate during the catalytic run.
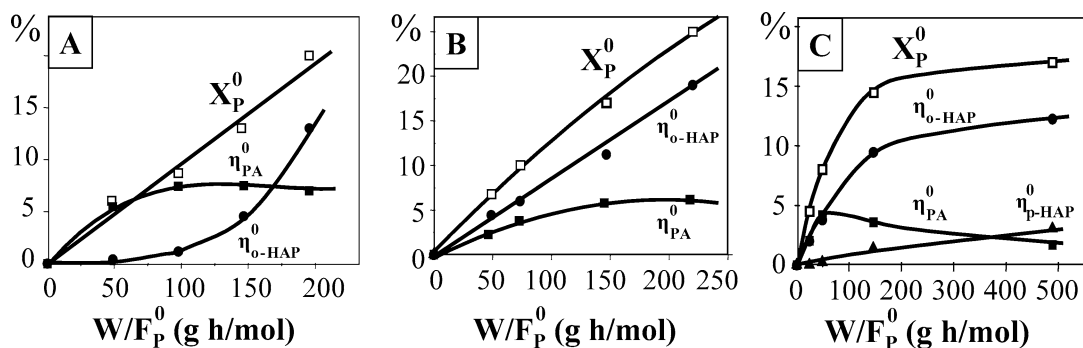
yjcat8348

C.L. Padró, C.R. Apesteguía / Journal of Catalysis 226 (2004) 308–320

Fig. 5. Product distribution for phenol/acetic acid reactions on: (A) HPA/C; (B) ZSM5; (C) HY. Product yields (η_i^0) and phenol conversion (X_P^0) at $t = 0$ as a function of contact time [553 K, 101.3 kPa total pressure, P/AA = 1].
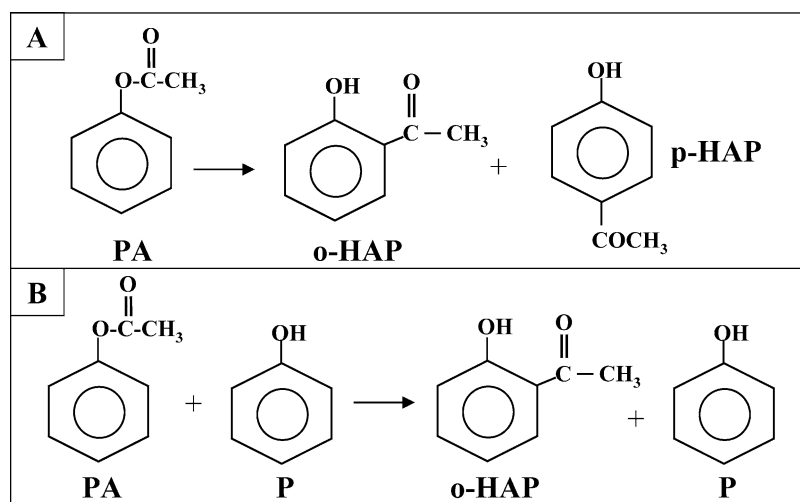
3.3. Reaction network

The effect of contact time on the product distribution was determined in order to identify primary and secondary reaction pathways. The observed deactivation, however, required that each data point be obtained on a fresh catalyst and that initial product yields be obtained by extrapolating to initial time on stream using semilogarithmic plots. The product yields at $t = 0$ (η_i^0) and the corresponding phenol conversion values on HPA/C are shown as a function of contact time in Fig. 5A. The local slopes of the curves in Fig. 5A give the rate of formation of each product at a specific phenol conversion and residence time. The nonzero initial slope for PA shows that it forms directly from the acylation of phenol with acetic acid. PA yield increases with increasing W/F_P^0 but reaches a maximum value as it converts to larger acylation products in secondary reactions with increasing space time. The initial zero slope of the o-HAP yield curve is consistent with o-HAP formation from conversion of primary PA products. Formation of p-HAP on HPA/C was not significant in the W/F_P^0 range studied. Fig. 5B shows the η_i^0 vs W/F_P^0 plot obtained on ZSM5. In contrast with results obtained on HPA/C, formation of o-HAP on ZSM5 displays a nonzero initial slope, thereby suggesting the direct C-acylation of phenol to o-HAP. The PA yield curve shows an initial nonzero slope and then reaches a maximum, indicating that PA is formed by direct O-acylation of phenol and then is converted to secondary products. p-HAP is formed in very small amounts on ZSM5. From the initial slopes of the yield curves in Fig. 5B we determined the initial formation rates of o-HAP and PA, respectively, and obtained $r_{o\text{-HAP},0}^0 = 2.43 \times 10^{-3}$ mmol/(h m²) and $r_{PA,0}^0 = 1.80 \times 10^{-3}$ mmol/(h m²) ($r_{i,0}^0$, is the formation rate of product i at $X_P \to 0$ and $t = 0$). Thus, on ZSM5 the direct C-acylation rate of phenol to o-HAP is higher than the O-acylation rate of phenol to PA. In a previous work using zeolite ZSM5 of Si/Al = 40 and under experimental conditions similar to those in the present work, Neves et al. [17] found that O-acylation of phenol to the PA pathway was favored compared to that of C-acylation of phenol to o-HAP. Qualitatively, zeolite HY showed similar evolutions of η_{PA}^0
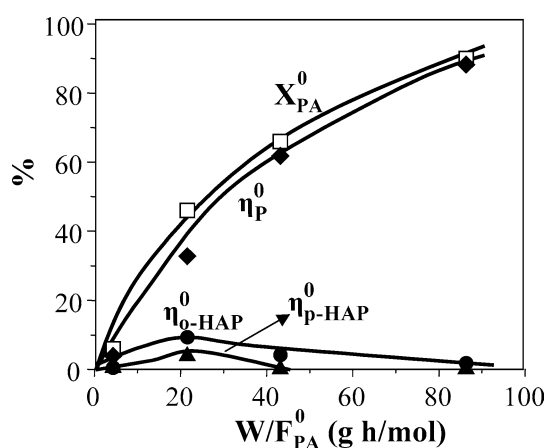
and $\eta_{o\text{-HAP}}^0$ with space time than zeolite ZSM5 (Fig. 5C). Initial formation rates of o-HAP and PA were similar on HY sample, i.e., $r_{o\text{-HAP},0}^0 \cong r_{PA,0}^0 \cong 1.24 \times 10^{-3}$ mmol/(h m²), but lower than on ZSM5. p-HAP was a secondary product formed on nonnegligible amounts on HY. In fact, $\eta_{p\text{-HAP}}^0$ increased with contact time and the selectivity to p-HAP for $W/F_P^0 = 500$ g h/mol was about 18%.

In order to gain more details on the reaction mechanism of phenol acylation with acetic acid, we studied the conversion of PA on ZSM5 ($T = 553$ K, $P = 101.3$ kPa, $P_{PA} = 0.638$ kPa). PA is the key intermediate to yield o-HAP from phenol by a consecutive two-step mechanism. The aim of this study was to investigate the direct transformation of PA to p- and o-HAP via a Fries rearrangement mechanism on zeolite ZSM5. Conversion of PA to p- and o-HAP isomers by Fries rearrangement involves the intramolecular migration of the acyl group to the *para*- and *ortho*-positions of the aromatic ring, respectively (Scheme 2A). The product yields at $t = 0$ and the corresponding PA conversion values on ZSM5 are shown as a function of contact time in Fig. 6. PA was essentially converted to phenol. The total selectivity to o- and p-HAP isomers reached about 28% for $X_{PA}^0 \cong 40\%$, which is consistent with previous results reported on acid zeolites [35,36], but rapidly decreased for higher X_{PA}^0 values and was negligible for $X_{PA}^0 = 80\%$, probably because of consecutive transformation of both isomers. Besides, a rapid activity decay for o-HAP formation was observed in contrast with the high stability that ZSM5 showed for the *ortho*-isomer synthesis from phenol and AA in Fig. 4B. We conclude then that the gas-phase formation of o-HAP from PA via a Fries rearrangement is not a significant reaction pathway on ZSM5.

Finally, to obtain further insight on the P/AA acylation mechanism an additional catalytic test was carried out on ZSM5 by cofeeding phenol with PA (553 K, $P = 101.3$ kPa, $P_{PA} = P_P = 0.638$ kPa, $W/F_P^0 = 43.1$ g h/mol). In Fig. 7 we plotted the evolution of PA conversion and product selectivities as a function of time. Initially, PA is readily and selectively converted to o-HAP showing that ZSM5 efficiently catalyzes the acylation of phenol with PA. PA decomposes to phenol and forms simultaneously an acylium ion which in turns attacks the phenol molecule to yield o-HAP

ARTICLE IN PRESS

S0021-9517(04)00288-X/FLA AID:8348 Vol.226(2)   yjcat8348   P.315 (308-320)
ELSGMLTM(YJCAT):m5 2004/05/28 Prn:28/06/2004; 13:34   by:Jolanta p. 8

C.L. Padró, C.R. Apesteguía / Journal of Catalysis 226 (2004) 308–320   315

Scheme 2. Phenyl acetate conversion reactions. (A) Fries rearrangement; (B) P/PA acylation.

Fig. 6. Product distribution for phenyl acetate conversion reactions on ZSM5. Product yields (η_i^0) and phenyl acetate conversion (X_{PA}^0) at $t = 0$ as a function of contact time [553 K, 101.3 kPa total pressure, $P_{PA} = 0.638$ kPa].
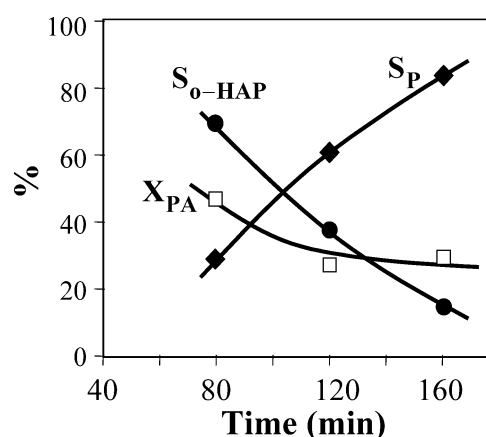
Fig. 7. Product distribution for phenol/phenyl acetate reactions on ZSM5. Selectivities (S_i) and phenyl acetate conversion (X_{PA}) as a function of time on stream [553 K, 101.3 kPa total pressure, $P_{PA} = P_P = 0.638$ kPa, $W/F_P^0 = 43.1$ g h/mol].

(Scheme 2B). However, Fig. 7 also shows that the *o*-HAP formation rate from P/PA acylation rapidly diminishes on stream despite that ZSM5 is highly stable for forming *o*-HAP from P/AA acylation (Fig. 4B).

Results of Figs. 5–7 allow us to propose the reaction network for the synthesis of *o*-HAP from the acylation of phenol with AA described in Scheme 3. Phenol initially reacts with AA via two parallel acylation reactions: by O-acylation phenol is transformed to PA and by C-acylation yields directly *o*-HAP. Formation of *o*-HAP also takes place via secondary reactions from PA, either by Fries rearrangement or by P/PA acylation. Regarding the production of *p*-HAP, only zeolite HY formed *p*-HAP, but as a minor product (Table 3) and via secondary reaction pathways (Fig. 5C). Neves et al. [17] have proposed that *p*-HAP on acid zeolites is formed through hydrolysis of *p*-acetoxyacetophenone resulting from the selective autoacylation of phenyl acetate. The relative rate of the different pathways involved in Scheme 3 greatly depends on the solid acid employed. In this regard, we dis-

cuss below the surface acidity requirements for the efficient catalysis of reaction steps leading from phenol to *o*-HAP.

3.4. Surface acid property and catalytic performance

The acylating agent or acylium ion CH_3CO^+ is formed on our solid acids from AA either on Brønsted or Lewis acid sites, as depicted in Scheme 4. Generated electrophilic CH_3CO^+ may then attack the phenol molecule either by electrophilic substitution of the *ortho*-hydrogen in the aromatic ring forming *o*-HAP or, alternatively, by O-acylation of the OH group producing PA. Results in Fig. 5A showed that on the HPA/C sample, which contains only surface Brønsted sites, phenol is initially converted exclusively to PA. This is explained by considering that on strong Brønsted acid sites of HPA-based catalysts the phenol molecule essentially interacts via the benzene ring [37], adopting a position parallel to the surface and favoring the attack of

ARTICLE IN PRESS

S0021-9517(04)00288-X/FLA   AID:8348   Vol.226(2)
ELSGMLTM(YJCAT):m5 2004/05/28 Prn:28/06/2004; 13:34

yjcat8348

P.316(308-320)
by:Jolanta p. 9

C.L. Padró, C.R. Apesteguía / Journal of Catalysis 226 (2004) 308–320
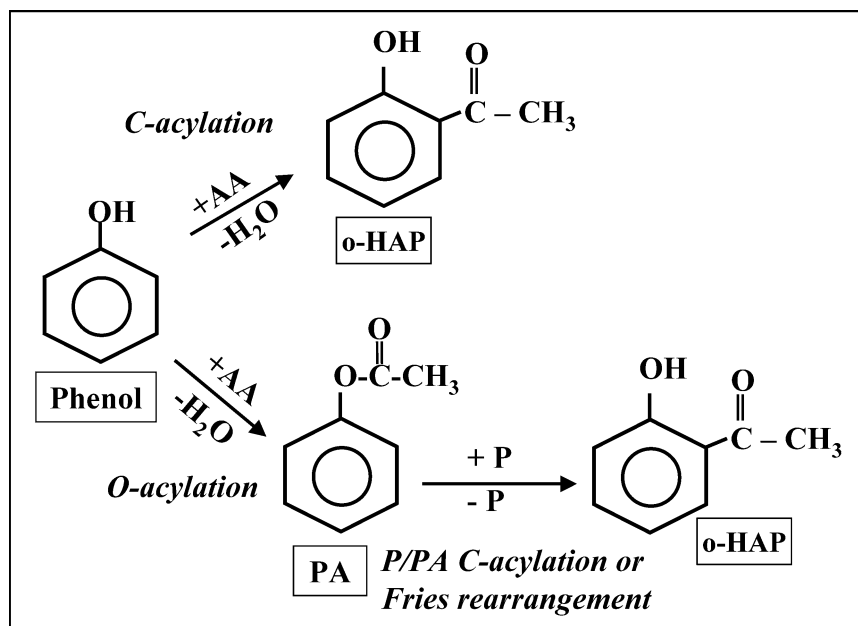
Scheme 3. Reaction network for the synthesis of o-HAP from phenol and acetic acid on solid acids.
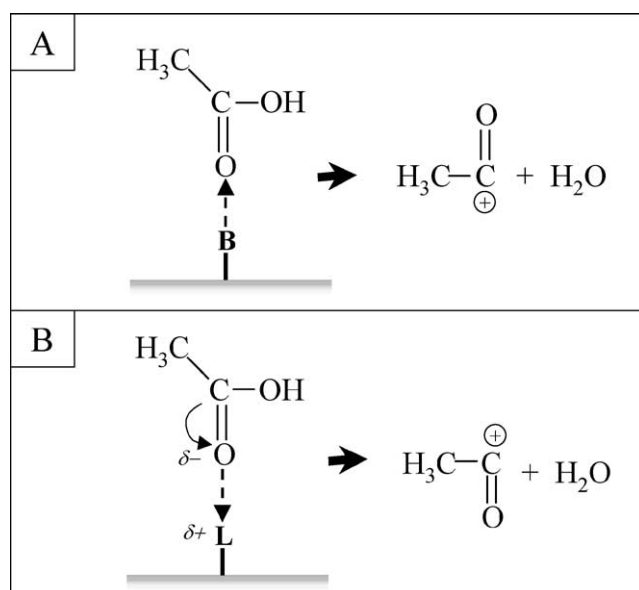
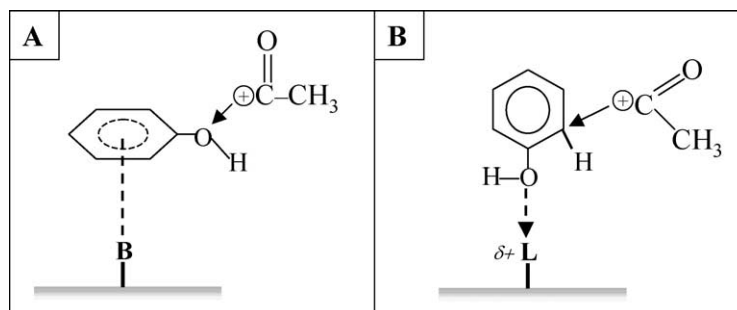Scheme 4. Formation of the acylating agent on: (A) Brønsted acid sites, (B) Lewis acid sites.

acylium ion mainly to the oxygen of phenol, as shown in Scheme 5A.

On zeolites ZSM5 and HY both o-HAP and PA are primary products (Fig. 5), but phenol is directly converted to o-HAP at higher (ZSM5) or similar (HY) rates than to PA. Zeolite NaY that contains only Lewis acid sites produces o-HAP with more than 60% selectivity for a phenol conversion of about 16%, similarly to the values found on zeolites HY and ZSM5, which contain similar Lewis acid site concentrations than NaY but L/B ratios between 1 and 1.5 (Table 2). These results suggest that C-acylation of phenol to yield o-HAP takes place mainly on surface Lewis

acid sites, probably as shown in Scheme 5B. As proposed by other authors [37,38], phenol is adsorbed on Lewis acid centers predominantly in vertical orientation and allows the electrophilic attack of benzene rings in the ortho-position, because stabilization of the ortho-isomer intermediate is favored as compared to the intermediate formation in the para-position [17]. This is consistent with the fact that we never observed the direct formation of p-HAP from phenol on the samples used in this work.

PA is consecutively converted to o-HAP on HPA/C, and zeolites HY and ZSM5 samples (Fig. 5). After formation and activation on Brønsted acid sites [35], PA may be transformed in o-HAP either by intramolecular Fries rearrangement or by its decomposition and consecutive phenol acylation (Scheme 6, intermolecular acylation). Our results show that on zeolite ZSM5 the conversion of PA to o-HAP via a Fries rearrangement is not a significant reaction pathway (Fig. 6). We must conclude then that on ZSM5, and probably on zeolite HY, PA decomposes to phenol and acylium ions which consecutively react and yield o-HAP by intermolecular C-acylation on Lewis acid sites, as described in Scheme 6. In contrast, HPA-based catalysts would convert PA to o-HAP essentially via an intramolecular Fries rearrangement on strong Brønsted acid sites (Scheme 6) because, as noted above, HPA catalysts do not promote the acylation intermolecular pathway to obtain o-HAP by C-acylation of phenol.

In summary, catalysts containing Lewis and Brønsted acid sites such as zeolites ZSM5 and HY exhibit a superior performance for producing o-HAP because they efficiently promote the two main reaction pathways leading from phenol to o-HAP, i.e., the direct C-acylation of phenol, and the O-acylation of phenol forming PA intermediates which

ARTICLE IN PRESS

S0021-9517(04)00288-X/FLA AID:8348 Vol.226(2)
ELSGMLTM(YJCAT):m5 2004/05/28 Prn:28/06/2004; 13:34

yjcat8348

P.317 (308-320)
by:Jolanta p. 10

C.L. Padró, C.R. Apesteguía / Journal of Catalysis 226 (2004) 308–320

317

Scheme 5. O- and C-acylation of phenol on Brønsted (A) and Lewis (B) acid sites, respectively.
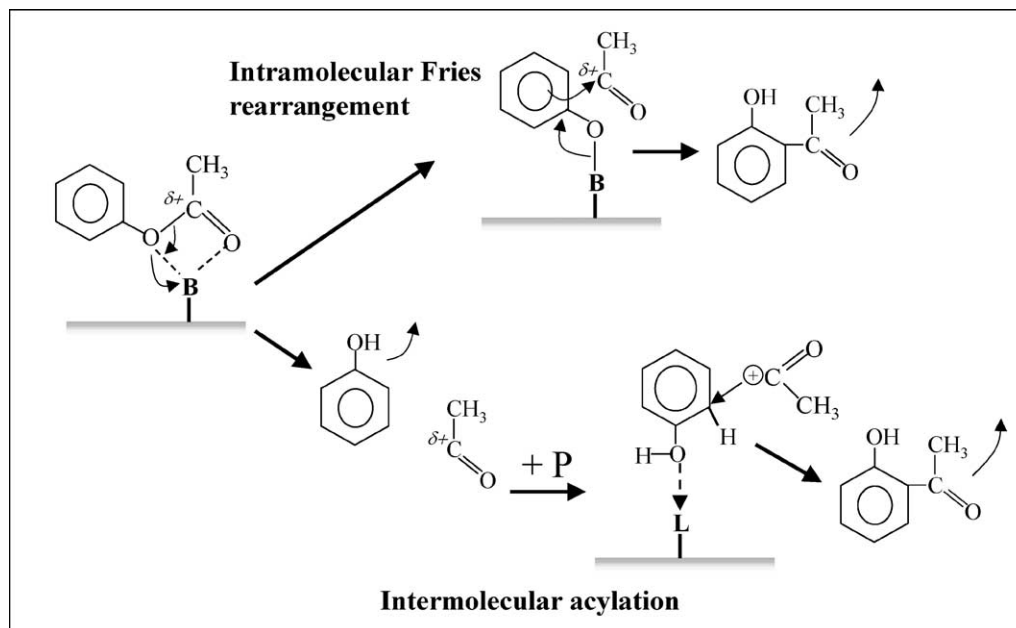
Scheme 6. Formation of *o*-HAP from PA via different reaction pathways.

are consecutively transformed via intermolecular P/PA C-acylation.

3.5. Catalyst deactivation

Data in Table 3 show that although phenol conversion remains practically constant on stream during the acylation of phenol with AA, the selectivity to PA rapidly increases at the expense of *o*-HAP over all the catalysts, except zeolite ZSM5. In Fig. 8 we have plotted the evolution of the activity *a* for the formation of *o*-HAP as a function of time on stream. The activity *a* is defined as $a = r_{o\text{-}HAP}/r^0_{o\text{-}HAP}$, where $r_{o\text{-}HAP}$ and $r^0_{o\text{-}HAP}$ are the formation rates of *o*-HAP at times *t* and zero, respectively. Fig. 8 shows that *a* does not change with time on ZSM5, but rapidly decreases on the other samples, particularly on samples HY and HPA/MCM-41.

Coke formed on ZSM5, Al-MCM-41, HY, SiO₂–Al₂O₃, and HPA/MCM-41 was determined by analyzing the samples after the catalytic tests by temperature-programmed oxidation. The resulting TPO profiles are shown in Fig. 9. The evolved CO_2 from HPA/MCM-41 gave rise to a well-defined
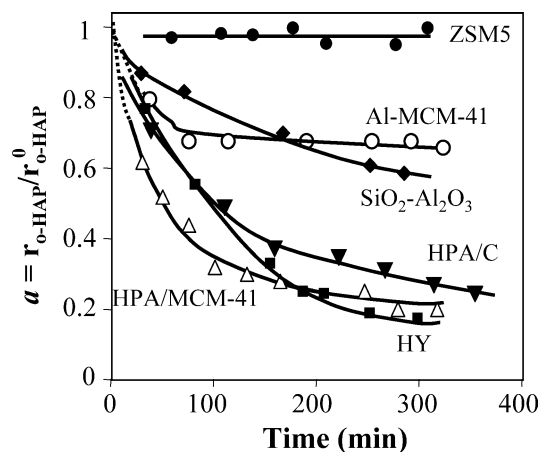
Fig. 8. Acylation of phenol with acetic acid: Activity (*a*) for *o*-HAP formation as a function of time [553 K, 101.3 kPa total pressure, $W/F^0_P = 146$ g h/mol, P/AA = 1, N₂/(P + AA) = 45].

TPO peak with a maximum at about 795 K. The TPO profile for zeolite HY showed that CO_2 evolves in a broad band between 600 and 1000 K, containing three overlapping peaks.

ARTICLE IN PRESS

S0021-9517(04)00288-X/FLA   AID:8348   Vol.226(2)
ELSGMLTM(YJCAT):m5 2004/05/28 Prn:28/06/2004; 13:34

yjcat8348

P.318 (308-320)
by:Jolanta p. 11

318   C.L. Padró, C.R. Apesteguía / Journal of Catalysis 226 (2004) 308–320
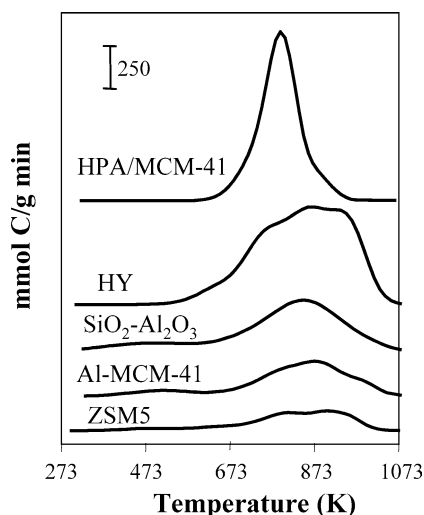
Fig. 9. Acylation of phenol with acetic acid. Temperature-programmed oxidation of the catalysts after the 6 h runs. 10 K/min heating rate.
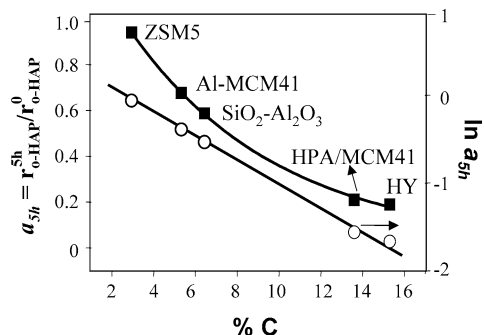

Fig. 10. Activity for o-HAP formation at 5 h on stream ($a_{5\,h}$) as a function of the amount of carbon formed during acylation of phenol with acetic acid.

Coke burnt on zeolite ZSM5 was qualitatively similar to that of zeolite HY, but the amount of CO_2 evolved from ZSM5 was significantly lower. Finally, the curves of CO_2 evolved from the oxidation of coke formed on samples Al-MCM-41 and SiO_2–Al_2O_3 were qualitatively similar and both presented a maximum at about 870 K.

The amount of carbon on the samples was measured from the area under the curves of Fig. 9 and the values ranged from 29.4 mg C/g catalyst on ZSM5 to 153 mg C/g on HY. In Fig. 10 we plotted the activity for the formation of o-HAP at 5 h on stream ($a_{5\,h} = r^{5\,h}_{o\text{-HAP}}/r^0_{o\text{-HAP}}$) during the acylation of phenol with AA as a function of the amount of carbon on the sample determined from Fig. 9. It is observed that $a_{5\,h}$ decreases with the amount of carbon on the sample, thereby suggesting that the activity decay for the formation of o-HAP is caused by coke formation. Fig. 10 also shows that $\ln a_{5\,h}$ vs %C is a linear plot, suggesting that the o-HAP formation rate diminishes exponentially with the amount of carbon formed on the samples.

In an attempt to obtain insight on the species responsible for coke formation we quantitatively evaluated the effect that varying space time W/F^0_P (and consequently X^0_P) has on o-HAP formation rate decay by determining the initial catalyst
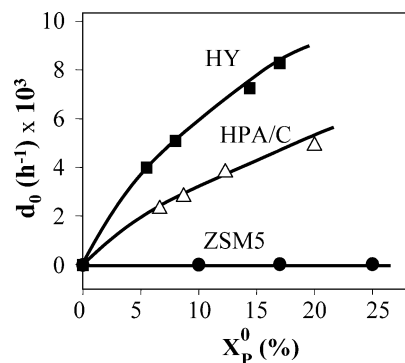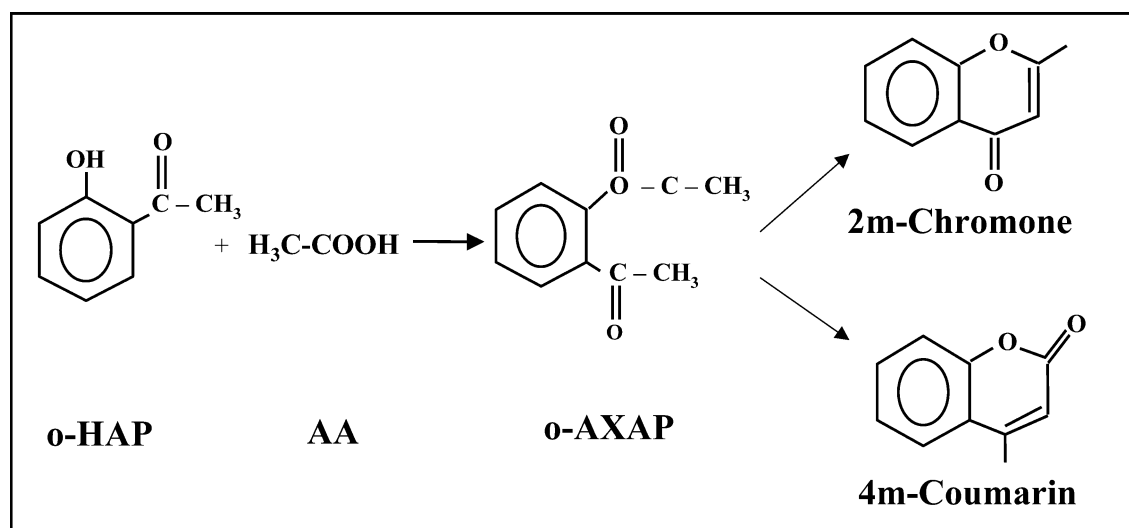

Fig. 11. Initial deactivation of o-HAP formation rate, $d_0 = -(da/dt)_{t=0}$, as a function of conversion of phenol at $t = 0$ on HY, ZSM5, and HPA/C samples. Acylation of phenol with acetic acid [553 K, 101.3 kPa total pressure, P/AA = 1, N_2/(P + AA) = 45].

deactivation, $d_0(h^{-1}) = -(da/dt)_{t=0}$, as the initial slope of the activity versus time curves obtained for different W/F^0_P values on HY, HPA/C, and ZSM5 samples. The resulting d_0 values are represented as a function of X^0_P in Fig. 11. Zeolite ZSM5 does not deactivate by increasing the conversion of phenol up to 25%, but on HPA/C and HY samples d_0 increases with X^0_P, thereby suggesting that coke is formed via consecutive side reactions from the products of the reaction.

As noted previously, zeolite ZSM5 does not deactivate during the acylation of phenol with AA (Fig. 4B), despite that it rapidly deactivates when PA or a P + PA mixture is used as reactants (Fig. 7). This is explained by taking into account that in the case that PA is added alone or in a P + PA mixture, the conversion of PA to P occurs with simultaneous formation of ketenes (CH_2=C=O) which are extremely reactive and unstable compounds that dimerize to diketenes and polymerize very quickly [39]. As a matter of fact, the formation of ketenes is the main reason of the significant catalyst activity decay observed during the liquid-phase Fries rearrangement of PA on solid acids [10]. In contrast, the acylation of phenol with AA produces concomitantly water (Schemes 3 and 4) and any consecutive formation of ketenes from PA is neutralized by the presence of moisture. In fact, water rapidly reacts with ketenes to produce acetic acid [40] and thereby suppresses the reaction pathway forming coke from ketene precursors. Thus, we conclude that because of the presence of water in the reaction products, ketenes are not responsible for the catalyst activity decay shown in Fig. 8 for zeolite HY and HPA/C.

Finally, we studied the effect that feeding o-HAP alone or in a o-HAP + AA mixture has on catalyst deactivation using SiO_2–Al_2O_3 and ZSM5 samples. o-HAP was fed on SiO_2–Al_2O_3 for 4 h ($T = 553$ K, $P_{o\text{-HAP}} = 0.45$ kPa, $W/F^0_{o\text{-HAP}} = 580$ g h/mol). We did not detect the formation of any product from o-HAP and the amount of coke formed after 4 h on stream was not significant (%C = 1.2). It seems that o-HAP is not strongly adsorbed on SiO_2–Al_2O_3 and does not form heavier products either. Thus, o-HAP would not be responsible by itself for the catalyst activity decay measured on SiO_2–Al_2O_3 in Fig. 8. The coinjection of o-HAP with

ARTICLE IN PRESS

S0021-9517(04)00288-X/FLA AID:8348 Vol.226(2)
ELSGMLTM(YJCAT):m5 2004/05/28 Prn:28/06/2004; 13:34

yjcat8348

P.319(308-320)
by:Jolanta p. 12

C.L. Padró, C.R. Apesteguía / Journal of Catalysis 226 (2004) 308–320

319

Scheme 7. Formation of coke precursors from *o*-HAP/AA conversion reactions.

AA ($T = 553$ K, $P_{AA} = 1.8$ kPa, $P_{o\text{-HAP}} = 0.45$ kPa) on SiO$_2$–Al$_2$O$_3$ formed phenol and two heavy unknown products. A rapid activity decay was observed and after 4 h on stream the amount of carbon deposited was 13.5%. This observed SiO$_2$–Al$_2$O$_3$ deactivation is consistent with results reported by Jayat and co-workers [17]. These authors, in fact, found that coke formed on MFI zeolites during the acylation of phenol with AA is mainly constituted by methylnaphthols, 2-methylchromone, and 4-methylcoumarin. Formation of 2m-cromone and 4m-coumarin may take place from *o*-HAP and AA as depicted in Scheme 7, via the initial formation of *o*-acetoxyacetophenone. In contrast, on ZSM5 we did not observe any catalyst deactivation by cofeeding *o*-HAP with AA and the amount of coke formed after 4 h of stream was only 1.5%. Besides, on ZSM5 we did not detect the formation of heavy compounds among the reaction products (the only reaction products were PA and phenol). These later results strongly suggest that on ZSM5 the formation of coke precursors via the reaction shown in Scheme 7 does not take place, probably because the narrow pore-size structure of ZSM5 hinders the formation of condensed intermediate compounds, such as *o*-AXAP.

4. Conclusions

Gas-phase acylation of phenol with acetic acid on solid acids produces essentially *o*-hydroxyacetophenone and phenyl acetate, together with minor amounts of *p*-hydroxyacetophenone, but the product formation rates, the reaction mechanism, and the catalyst activity decay greatly depend on the surface acid site density and strength of the solids. HPA-based catalysts, such as HPA/C or HPA/MCM-41, that contain only strong Brønsted acid sites, promote exclusively the O-acylation of phenol forming phenyl acetate which is then consecutively transformed to *o*-HAP, probably via an intramolecular Fries rearrangement. Samples containing

Lewis acid sites promote also the direct C-acylation of phenol in the *ortho*-position to yield *o*-HAP. Zeolites ZSM5 and HY, which contain strong Lewis and Brønsted acid sites, produce *o*-HAP at high rates because they efficiently catalyze the two main reaction pathways leading from phenol to *o*-HAP, i.e., the direct C-acylation of phenol and the O-acylation of phenol forming the PA intermediate which is consecutively transformed via intermolecular phenol/PA C-acylation. Solid acids of moderate acid strength such as Al-MCM-41 or SiO$_2$–Al$_2$O$_3$ are less active and selective for *o*-HAP formation than zeolites HY or ZSM5.

All the samples used in this work, except zeolite ZSM5, rapidly deactivate on stream because of coke formation. Coke precursors are formed from secondary condensation reactions, probably between *o*-HAP and acetic acid, and not from any ketene formation by phenyl acetate decomposition. The superior stability of zeolite ZSM5 is explained by considering that its narrow pore-size structure hampers the formation of coke precursor compounds.

Acknowledgments

References

[1] J. Fritch, O. Fruchey, T. Horlenko, US patent 4954652, Hoechst Celanese Corporation (1990).
[2] I. Uwaydah, M. Aslam, C. Brown, S. Fitzhenry, J. McDonough, US patent 5696274 (1997).
[3] M.J. Climent, A. Corma, S. Iborra, J. Primo, J. Catal. 151 (1995) 60.

[4] M.T. Drexler, M.D. Amiridis, J. Catal. 214 (2003) 136.

[5] K.G. Davenport, Ch.B. Hilton, US patent 4524217, Celanese Corp. (1985).

[6] A. Commarieu, W. Hölderich, J.A. Laffitee, M. Dupont, J. Mol. Catal. A: Chem. 182 (2002) 137.

[7] C.S. Cundy, R. Higgins, S.A. Kibby, B.M. Lowe, R.M. Paton, Tetrahedron Lett. 30 (1989) 2281.

[8] A. Vogt, H. Kouwenhoven, R. Prins, Appl. Catal. 123 (1995) 37.

[9] F. Jayat, M.J. Sabater Picot, M. Guisnet, Catal. Lett. 41 (1996) 181.

[10] A. Heidekum, M.A. Harmer, W.F. Hölderich, J. Catal. 176 (1998) 260.

[11] E.F. Kozhevnikova, J. Quartararo, I.V. Kozhevnikov, Appl. Catal. A 245 (2003) 69.

[12] J. Mueller, W. Wiersdorff, W. Kirschenlohr, G. Schwantje, US patent 4508924, BASF (1985).

[13] G.N. Mott, US patent 4607125, Celanese Corporation, 1986.

[14] M. Guisnet, D.B. Lukyanov, F. Jayat, P. Magnoux, I. Neves, Ind. Eng. Chem. Res. 34 (1995) 1624.

[15] B.B. Gupta, US patent 4668826, Celanese Corporation, 1987.

[16] K.G. Bhattacharyya, A.K. Talukdar, P. Das, S. Sivasanker, Catal. Commun. 2 (2001) 105.

[17] I. Neves, F. Jayat, P. Magnoux, G. Perot, F.R. Ribeiro, M. Gubelman, M. Guisnet, J. Mol. Catal. 93 (1994) 169.

[18] F. Jayat, M. Guisnet, M. Goldwasser, G. Giannetto, Stud. Surf. Sci. Catal. 105 (1997) 1149.

[19] Y.V. Subba Rao, S.J. Kulkarni, M. Subrahmanyam, A.V. Rama Rao, Appl. Catal. A 133 (1995) L1.

[20] K.J. Edler, J.W. White, Chem. Mater. 9 (1997) 1226.

[21] I.V. Kozhenikov, K.R. Kloestra, A. Sinnema, H.W. Zandbergen, H. van Bekkum, J. Mol. Catal. A: Chem. 114 (1996) 287.

[22] J.A. Lercher, Ch. Gründlig, G. Eder-Mirth, Catal. Today 27 (1996) 353.

[23] P.A. Jacobs, R. von Ballmoos, J. Phys. Chem. 86 (1982) 3050.

[24] M.T. Aronson, R.J. Gorte, W.E. Farneth, J. Catal. 105 (1987) 455.

[25] A. Corma, V. Fornés, F. Rey, Zeolites 13 (1993) 56.

[26] A. Boréave, A. Aroux, C. Guimon, Micropor. Mater. 11 (1997) 275.

[27] E.P. Parry, J. Catal. 2 (1963) 371.

[28] J.W. Ward, J. Catal. 10 (1968) 34.

[29] H. Knözinger, Adv. Catal. 25 (1976) 184.

[30] J. Wang, L. Huang, H. Chen, Q. Li, Catal. Lett. 55 (1998) 157.

[31] A. Sakthivel, S.E. Dapurkar, N.M. Gupta, S.K. Kulshreshtha, P. Selvam, Micropor. Mesopor. Mater. 65 (2003) 177.

[32] G. Busca, Catal. Today 41 (1998) 191.

[33] R.A. Beyerlin, G.B. Mc Vicker, L.N. Yacullo, J.J. Ziemak, J. Phys. Chem. 92 (1988) 1967.

[34] G.I. Woolery, G.H. Kuehl, H.C. Timken, A.W. Chester, J.C. Vartuli, Zeolites 19 (1997) 288.

[35] V. Pouilloux, J.-P. Bodibo, I. Neves, M. Gubelmann, G. Perot, M. Guisnet, in: M. Guisnet, et al. (Eds.), Heterogeneous Catalysis and Fine Chemicals II, Elsevier, Amsterdam, 1991, p. 513.

[36] V. Borzatta, G. Busca, E. Poluzzi, V. Rossetti, M. Trombetta, A. Vaccari, Appl. Catal. A 257 (2004) 85.

[37] K.V.R. Chary, K. Ramesh, G. Vidyasagar, V.V. Rao, J. Mol. Catal. A: Chem. 198 (2003) 195.

[38] K. Tanabe, T. Nishizaki, in: G.C. Bond, P.B. Wells, F.C. Tompkins (Eds.), Proceedings of the Sixth International Conference on Catalysis, vol. 2, The Chemical Society, London, 1977, p. 863.

[39] T.T. Tidwell, Acc. Chem. Res. 23 (1990) 273.

[40] E. Bothe, A.M. Dessouki, D. Schulte-Frohlinde, J. Phys. Chem. 84 (1980) 3270.